A Multi-Scale Topological Shape Model for Single and Multiple Component Shapes

Padraig Corcoran

School of Computer Science & Informatics
Cardiff University, Wales, UK.

Joviša Žunić

Mathematical Institute, Serbian Academy of Sciences, Serbia.

Paul L. Rosin

School of Computer Science & Informatics
Cardiff University, Wales, UK.

Abstract

A novel shape model of multi-scale topological features is proposed which considers those features relating to connected components and holes. This is achieved by considering the *persistent homology* of a pair of sublevel set functions corresponding to a pair of distance functions defined on the ambient space. The model is applicable to both single and multiple component shapes and, to the authors knowledge, is the first shape model to consider multi-scale topological features of multiple component shapes. It is demonstrated, both qualitatively and quantitatively, that the proposed model models useful multi-scale topological features and outperforms a commonly used benchmark models with respect to the task of multiple component shape retrieval.

Keywords: Multiple Component Shapes, Topology, Multi-Scale, Persistent Homology

Email address: corcoranp@cardiff.ac.uk (Padraig Corcoran)

1. INTRODUCTION

Shape modelling is a fundamental research problem with many applications including modelling the shape of a human skull toward performing facial reconstruction [1], modelling the shape of the right proximal femur toward predicting the risk factor for incident hip fracture [2] and modelling the shape of objects in a warehouse toward performing warehouse automation [3].

There exist some general shape models that can produce an arbitrarily large number of descriptors, and the two main instances are Fourier descriptors and moments. Each of these have spawned many alternative developments, e.g. Elliptic Fourier descriptors [4], UNL-Fourier descriptors [5] for the former, and geometric moments, Zernike moments, Legendre moments, Chebyshev moments, etc. [6, 7] for the latter. On the other hand, there exist many specific shape models which attempt to model only a specific feature of shape. Such features include convexity [8], ellipticity, rectangularity, and triangularity [9]. In addition, there are also many shape representations that provide generic signatures. While their interpretation is not as intuitive as the simple global descriptors such as convexity, etc., they are convenient for matching although their representation is often not compact. Examples include shape context [10], curvature scale space [11], axis-based features [12], autoregressive model [13], chord length distributions [14].

In this paper we propose a novel shape model which models multiscale topological features. Modelling topological features has many applications such as modelling articulated objects in a manner which is invariant to changes in object pose. Although scale is not a topological concept, different topological features can appear and disappear at different scales and therefore a multi-scale approach to modelling is required. To illustrate this requirement consider the three shapes displayed in Figure 1. The shape in Figure 1(a) consists of two larger scale connected components connected by a smaller scale path. On the other hand, the shape in Figure 1(b) consists of a single larger scale connected component. Therefore, from a multi-scale perspective the topological features

(a) (b) (c)

Figure 1: Three single component shapes with distinct multi-scale topological features are displayed in (a), (b) and (c).

of these shapes can be considered distinct. The shape in Figure 1(c) consists of a single connected component which surrounds a larger scale region. Therefore, from a multi-scale perspective the topological features of this shape can be considered distinct from the previous two shapes. If a multi-scale perspective is not considered then the above shape distinctions cannot be made, and instead all shapes will be considered to have identical topological features. That is, from a non multi-scale perspective all three shapes consist of a single connected component.

Modelling multiple component shapes, which consist of one or more connected components, is an emerging field of research with many applications such as modelling textures consisting of multiple repeating elements [15]. The shape model proposed in this paper is applicable to both single and multiple component shapes. To illustrate the requirement for a multi-scale approach to modelling topological features of multiple component shapes consider the three shapes displayed in Figure 2. The shape in Figure 2(a) consists of two larger scale connected components which slightly overlap to form a single connected component. The shape in Figure 2(b) consists of two larger scale connected components which are spatially close but do not overlap. Therefore, from a multi-scale perspective the topological features of these shapes can be considered similar. The shape in Figure 2(c) consists of two larger scale path-connected components which are spatially far apart. Therefore, from a multi-scale perspective the topological features of this shape can be considered distinct from the

(a) (b) (c)

Figure 2: Three multiple component shapes with distinct multi-scale topological features are displayed in (a), (b) and (c).

previous two shapes. If a multi-scale perspective is not considered the above shape distinctions cannot be made. Instead the shapes in Figures 2(b) and 2(c) will be considered to have identical topological features while the shape in Figure 2(a) will be considered to have distinct topological features.

There exist a number of classes of topological features one could consider when attempting to model single and multiple component shapes such as the Euler characteristic and Homotopy groups. However, these features do not provide any means of modelling multi-scale topological features. The shape model proposed in this paper employs a set of topological features known as *persistent homology* which does provide a means of modelling multi-scale topological features [16]. A consequence of this fact is that the proposed shape model is capable of making the multi-scale distinctions between the shapes illustrated in Figures 1 and 2.

Before computing the persistent homology of a given shape one must first compute a *filtration* which is a sequence of representations of the shape indexed by a scale parameter. Given a filtration the corresponding persistent homology determines the topological features which exist in the filtration plus the corresponding scales at which each appeared and subsequently disappeared. This information is most commonly represented as a *persistence diagram* which is a multiset of points in the plane where each point (i, j) indicates that a particular topological feature appeared and subsequently disappeared at scales i and j respectively. The shape model proposed in this paper employs a novel

approach to constructing a pair of filtrations such that the corresponding persistent homology models useful multi-scale topological features. The model is distinct from existing shape models which employ persistent homology in the sense that filtrations are defined with respect to a triangulation of the ambient space. Using this approach features relating to distance in the ambient space, such as the distance between two components, can be modelled.

The layout of the remainder of this paper is as follows. Section 2 reviews the different classes of topological features one could consider when attempting to model the topological features of shape. Existing shape models which consider topological features are also reviewed in this section. Section 3 describes the proposed shape model. Section 4 presents a qualitative and quantitative evaluation of the proposed model with respect to single and multiple component shapes. Finally, section 5 draws conclusions from this work and presents some possible directions for future work.

2. Related Works

As discussed in the introduction to this article, there exist a number of classes of topological features one could consider when attempting to model single and multiple component shapes. Note that, in mathematical literature topological features are commonly referred to as topological invariants. The *Euler characteristic* is a topological feature equaling the alternating sum of the number of connected components and holes of different dimensions [17]. However this is a weak feature in the sense that it cannot discriminate between shapes with very distinct topological features. Furthermore, the Euler characteristic does not provide any means of modelling multi-scale topological features. The *Homotopy groups* are topological features which model information relating to connected components and holes of different dimensions. However these features do not provide any means of modelling multi-scale topological features. Neither the Euler characteristic or the Homotopy groups are capable of making the multi-scale distinctions between the shapes illustrated in Figures 1 and 2.

The *Homology groups* also model information relating to connected components and holes of different dimensions but in a slightly weaker sense than the Homotopy groups. However, these features can be generalised to provide a means of modelling multi-scale topological features. This generalisation is known as *persistent homology* and is employed by the shape model proposed in this paper. This model is capable of making the multi-scale distinctions between the shapes illustrated in Figures 1 and 2.

In the remainder of this section we review existing shape models which attempt to model topological features and focus particularly on those models which employ persistent homology. The shape model proposed in this paper is distinct from these in the sense that it defines filtrations on the ambient space as opposed to the shape itself [18]. Furthermore, the proposed model is applicable to both single and multiple component shapes. Although some existing models have the potential to be applied to multiple component shapes, their performance with respect to such shapes has not previously been considered.

Turner et al. [19] propose a shape model known as the *persistent homology transform*. This model computes a set of persistence diagrams where each corresponds to a filtration defined on the shape with respect to distance in a specified direction. The authors demonstrate the utility of their model with respect to modelling two dimensional shapes corresponding to generic objects and three dimensional shapes corresponding to animal bones. Curry et al. [20] later extended this model to determine the number of directions required to fully model the topological features of a given shape. Di Fabio et al. [21] propose a shape model capable of comparing shapes based on partial similarity that can compare partially occluded shapes. This model computes a persistence diagram corresponding to a filtration defined on the shape which considers the negative distance from a central point. The authors demonstrate the utility of their model with respect to modelling two and three dimensional shapes corresponding to generic objects. Di Fabio et al. [22] propose a shape model which employs two different filtrations defined on the shape. One filtration considers the distance to a vector pointing in a principle direction and passing through the mean point.

The other considers the distance to a plane orthogonal to this vector and passing through the mean point. The authors propose three different transformations of the persistence diagram to complex polynomials which allow similarly to be computed efficiently. The authors demonstrate the utility of their model with respect to modelling three dimensional shapes corresponding to generic objects. Zeppelzauer et al. [23] propose a shape model for three dimensional surfaces by first creating a depth map representation of the surface and then constructing a filtration defined on the surface. Cerri et al. [24] propose a method for approximating the distance between persistence diagrams in the context of shape analysis. The authors use three different filtrations considering distance to a principle line, distance to a principle plane and distance to a central point.

3. Topological Shape Model

This section describes the proposed shape model which is based on persistent homology and models multi-scale topological features. The model first computes a pair of filtrations corresponding to positive and negative distance functions which are in turn used to compute a pair of persistence diagrams. These persistence diagrams model the multi-scale topological features of a given shape.

The layout of this section is as follows. Section 3.1 briefly introduces background material on filtrations and persistent homology. Section 3.2 presents the formulation of the proposed shape model. Section 3.3 describes how the proposed model is implemented in the context of two dimensional image shape analysis.

3.1. Filtrations and Persistent Homology

This section briefly introduces background material on the filtrations and persistent homology. A more detailed introduction to these topics can be found in [25, 26].

An (abstract) simplicial complex $\mathcal{K}$ is a finite collection of sets such that for each $\sigma \in \mathcal{K}$ all subsets of σ are also contained in $\mathcal{K}$. Each element $\sigma \in \mathcal{K}$

is called a k-simplex where $k = |\sigma| - 1$ is the corresponding dimension of the simplex. The faces of a simplex σ correspond to all simplices τ where $\tau \subset \sigma$. The dimension of a simplicial complex $\mathcal{K}$ is the largest dimension of any simplex $\sigma \in \mathcal{K}$. Given a simplicial complex $\mathcal{K}$, the formal sum c defined by Equation 1 is called a p-chain where each $\sigma_i \in \mathcal{K}$ is a p-simplex and each λ_i is an element of a given field. For the purposes of this work we consider the field $\mathbb{Z}_2$ [27].

$$c = \sum \lambda_i \sigma_i \tag{1}$$

The vector space of all p-chains is denoted $C_p(\mathcal{K})$. The boundary map $\partial_p : C_p(\mathcal{K}) \to C_{p-1}(\mathcal{K})$ is the homomorphism defined by Equation 2 where $\hat{v_i}$ indicates the deletion of v_i from the sequence. The boundary of a p-simplex $\sigma = [v_0, \ldots, v_p]$ is equal to the sum of its $(p-1)$-dimensional faces.

$$\partial_p \sigma = \sum_{i=0}^{p} (-1)^i [v_1, \ldots, \hat{v_i}, \ldots, v_p] \tag{2}$$

The kernel of ∂_p is called the vector space of p-cycles and is denoted $Z_p(\mathcal{K})$. The image of ∂_p is called the vector space of p-boundaries and is denoted $B_p(\mathcal{K})$. The fact that $\partial_{p+1}\partial_p = 0$ implies that $B_p(\mathcal{K}) \subseteq Z_k(\mathcal{K})$. The quotient space $H_p(\mathcal{K}) = Z_p(\mathcal{K})/B_p(\mathcal{K})$ is called the p-homology group of $\mathcal{K}$. Intuitively an element of the p-homology group corresponds to a p-dimensional hole in $\mathcal{K}$. That is, an element of the 0-homology group corresponds to a path-connected component in $\mathcal{K}$ while an element of the 1-homology group corresponds to a one dimensional hole in $\mathcal{K}$. The rank of $H_p(\mathcal{K})$ is called the p-th Betti number and is denoted $\beta_p(\mathcal{K})$.

Given a simplicial complex $\mathcal{K}$ containing m simplices, consider a function $f : \mathcal{K} \to \mathbb{R}$ such that $f(\tau) \leq f(\sigma)$ whenever τ is a face of σ. For all $a \in \mathbb{R}$, the sublevel set $\mathcal{K}(a) = f^{-1}(-\infty, a]$ is a subcomplex of $\mathcal{K}$. The ordering of the simplices of $\mathcal{K}$ with respect to the values of f induces a *filtration* on the set of subcomplexes corresponding to sublevel sets defined in Equation 3.

$$\emptyset = \mathcal{K}_0 \subset \cdots \subset \mathcal{K}_{m-1} \subset \mathcal{K}_m = \mathcal{K} \tag{3}$$

Given a filtration $\mathcal{K}_0, \ldots, \mathcal{K}_{m-1}, \mathcal{K}_m$ of a simplicial complex $\mathcal{K}$, for every $i \leq j$ there exists an inclusion map from $\mathcal{K}_i$ to $\mathcal{K}_j$ and in turn an induced homomorphism from $H_p(\mathcal{K}_i)$ to $H_p(\mathcal{K}_j)$ for each dimension p. An element of the p-homology group is *born* at $\mathcal{K}_{i+1}$ if it exists in $H_p(\mathcal{K}_{i+1})$ but does not exist in $H_p(\mathcal{K}_i)$. An element of the p-homology group *dies* at $\mathcal{K}_{i+1}$ if it exists in $H_p(\mathcal{K}_i)$ but does not exist in $H_p(\mathcal{K}_{i+1})$. If an element of a p-homology group never dies, its death is determined to be at a simplicial complex $\mathcal{K}_\infty$.

An element of the p-homology group which is born at $\mathcal{K}_i$ and dies at $\mathcal{K}_j$ can be represented as a point (i, j) in the space $\{(i, j) \in \mathbb{R}^2, i \leq j\}$ with corresponding *persistence* value of $j - i$. If the filtration is indexed by a scale parameter, the magnitude of $j - i$ is a measure of the scale of the topological feature in question. For a given simplicial complex $\mathcal{K}$, the multiset of points corresponding to a p-homology group is called a p-dimensional *persistence diagram* and is denoted $\text{Pers}_p(\mathcal{K})$ [28].

As discussed above, in this work we consider the problem of modelling two dimensional shapes. In this context, one only needs to consider persistence diagrams corresponding to the 0- and 1-homology groups; that is, $\text{Pers}_0(\mathcal{K})$ and $\text{Pers}_1(\mathcal{K})$. All higher dimensional homology groups will equal the null set. This is a consequence to the fact that a two dimensional shape can only contain path-connected components and one dimensional holes; higher dimensional holes cannot exist.

In many situations it is necessary to compute a distance between a pair of persistence diagrams. A commonly employed distance is the q-Wasserstein distance which is defined as follows. Let $\mathcal{U}$ and $\mathcal{V}$ be two persistence diagrams for which we wish to compute the corresponding q-Wasserstein distance. To make the persistence diagrams stable, each (i, i) on the diagonal is counted with infinite multiplicity. The q-Wasserstein distance $W_q(\mathcal{U}, \mathcal{V})$ is then defined by Equation 4 where η ranges over all bijections and $\|u - v\|_\infty = \max\{|u|, |v|\}$. The task of computing $W_q(\mathcal{U}, \mathcal{V})$ can be reduced to bipartite graph matching

problem [29].

$$W_q(\mathcal{U}, \mathcal{V}) = \left[\inf_{\eta:\mathcal{U}\to\mathcal{V}} \sum_{u\in\mathcal{U}} \|u - \eta(u)\|_\infty^q \right]^{\frac{1}{q}} \tag{4}$$

3.2. Shape Model Formulation

This section presents the formulation of the proposed shape model. Let X be a compact subset in $\mathbb{R}^d$ for which we wish to model the corresponding multi-scale topological features. In the case of two dimensional shape modelling considered in this paper, the dimension d is equal to 2. The unsigned distance function $U : \mathbb{R}^d \to \mathbb{R}$ with respect to X is defined by Equation 5.

$$U(y) = \inf_{x\in X} \|x - y\| \tag{5}$$

Let $L_t^U = \{x : U \leq t\}$ denote the corresponding sublevel set function and $\text{Pers}_p(L_t^U)$ denote the persistence diagrams of a filtration which models this function. If X is a finite set of points in $\mathbb{R}^d$, such a filtration may be constructed by considering the Čech complex which equals the nerve of the set of balls of increasing radius centred at each point. $\text{Pers}_p(L_t^U)$ is a commonly employed model of multi-scale topological features [30]. As will be illustrated in the results section of this article, in many cases this model does not represent an accurate model of multi-scale topological features.

In this paper, we propose to overcome the above limitation by considering two distance functions $S^+ : \mathbb{R}^d \to \mathbb{R}$ and $S^- : \mathbb{R}^d \to \mathbb{R}$. These functions are defined in Equations 6 and 7 respectively where X^c denotes the complement of X.

$$S^+(y) = \inf_{x\in X} \|x - y\| \tag{6}$$

$$S^-(y) = \inf_{x\in X^c} \|x - y\| \tag{7}$$

We refer to these functions as positive and negative distance functions respectively. Note that, the positive distance function is equivalent to the unsigned

distance function. Let $L_t^{S^+} = \{x : S^+ \leq t\}$ and $L_t^{S^-} = \{x : S^- \leq t\}$ denote the sublevel set functions of S^+ and S^- respectively. In this work we model multi-scale topological features of X by considering the persistence diagrams of filtrations which model these functions. We denote these persistence diagrams as $\text{Pers}_p(L_t^{S^+})$ and $\text{Pers}_p(L_t^{S^-})$ respectively.

The persistence diagrams $\text{Pers}_p(L_t^{S^+})$ and $\text{Pers}_p(L_t^{S^-})$ corresponding to the shape of Figure 1(a) are displayed in Figures 3(a) and 3(b) respectively. The persistence diagrams $\text{Pers}_p(L_t^{S^+})$ and $\text{Pers}_p(L_t^{S^-})$ corresponding to the shape of Figure 1(b) are displayed in Figures 3(c) and 3(d) respectively. Note that these persistence diagrams discriminate between the shapes in question. That is, although the persistence diagrams $\text{Pers}_p(L_t^{S^+})$ corresponding to both shapes are equal, the persistence diagrams $\text{Pers}_p(L_t^{S^-})$ corresponding to both shapes are distinct. Specifically, $\text{Pers}_p(L_t^{S^-})$ in Figure 3(b) indicates the existence of a single element of the 0-homology group and two elements of the 1-homology group with significant persistence. On the other hand, $\text{Pers}_p(L_t^{S^-})$ in Figure 3(d) indicates the existence of a single element of the 0-homology group and a single element of the 1-homology group with significant persistence. The two elements of the 1-homology group with significant persistence in Figure 3(b) are a consequence of the fact that shape in question consists of two larger scale path-connected components connected by a smaller scale path.

3.3. Image Shape Model

In this section we describe how the proposed shape model is implemented in the context of two dimensional images of shapes. We assume the images in question are binary where pixel values of 0 and 1 correspond to foreground object and background respectively. Three such images are displayed in Figure 1.

For a given binary image I, the following approach was employed to construct filtrations which model the positive and negative distance functions. First a simplicial complex representation $\mathcal{K}$ of the image is constructed as follows. For each image pixel $p \in I$ a corresponding 0-simplex is included in $\mathcal{K}$. For each

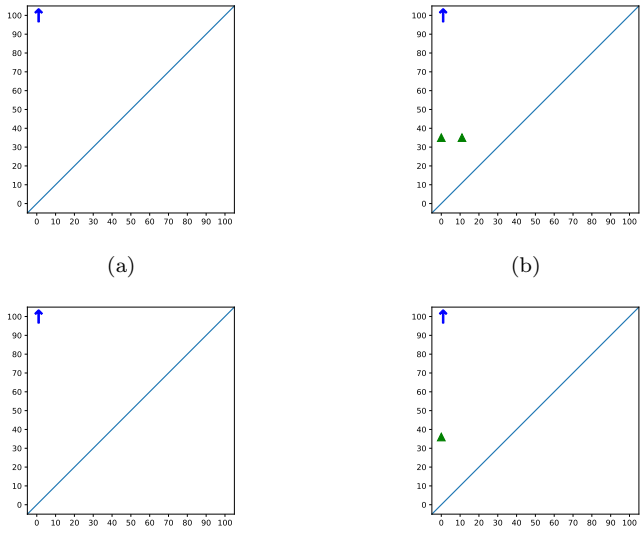

(a) (b)

(c) (d)

Figure 3: The persistence diagrams $\text{Pers}_p(L_t^{S^+})$ and $\text{Pers}_p(L_t^{S^-})$ corresponding to the shape of Figure 1(a) are displayed in (a) and (b) respectively. The persistence diagrams $\text{Pers}_p(L_t^{S^+})$ and $\text{Pers}_p(L_t^{S^-})$ corresponding to the shape of Figure 1(b) are displayed in (c) and (d) respectively. In each figure elements of $\text{Pers}_0(.)$ and $\text{Pers}_1(.)$ are represented using blue circles and green triangles respectively. Elements of $\text{Pers}_0(.)$ that appear but do not disappear are determined to disappear at a value of ∞ and are represented by a blue vertical arrow. Note that, each persistence diagram $\text{Pers}_0(.)$ in this figure contains zero elements. Hence, the figure contains zero blue circles.

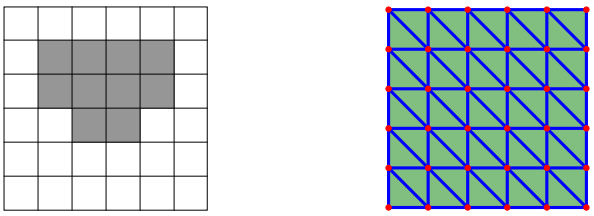

(a) (b)

Figure 4: A binary image of size 6×6 and corresponding simplicial complex representation $\mathcal{K}$ are displayed in (a) and (b) respectively. In (b) red dots represent 0-simplices, blue lines represent 1-simplices and green triangles represent 2-simplices.

1.4	1	1	1	1	1.4
1	0	0	0	0	1
1	0	0	0	0	1
1.4	1	0	0	1	1.4
2.2	1.4	1	1	1.4	2.2
2.8	2.2	2	2	2.2	2.8

(a)

0	0	0	0	0	0
0	1	1	1	1	0
0	1	1.4	1.4	1	0
0	0	1	1	0	0
0	0	0	0	0	0
0	0	0	0	0	0

(b)

Figure 5: The Euclidean distance transforms $d^+ : I \to \mathbb{R}$ and $d^- : I \to \mathbb{R}$ of the image I displayed in Figure 4(a) are displayed in (a) and (b) respectively.

pair of 0-simplices which are vertically, horizontally or main diagonal adjacent with respect to the corresponding image pixels, a corresponding 1-simplex is included in $\mathcal{K}$. For each triple of 0-simplices where all subsets of pairs are vertically, horizontally or main diagonally adjacent, a corresponding 2-simplex is included in $\mathcal{K}$. A small binary image and corresponding simplicial complex representation $\mathcal{K}$ are displayed in Figures 4(a) and 4(b) respectively.

Next, functions $f^+ : \mathcal{K} \to \mathbb{R}$ and $f^- : \mathcal{K} \to \mathbb{R}$ which induce filtrations modelling the positive and negative distance functions respectively are computed. Toward this goal the Euclidean distance transforms $d^+ : I \to \mathbb{R}$ and $d^- : I \to \mathbb{R}$, which are defined in Equations 8 and 9 respectively, are computed. Here $\|p-q\|$ denotes the Euclidean distance between the centroids of pixels p and q, $\text{Fore}(I)$ denotes the set of foreground pixels of I, and $\text{Back}(I)$ denotes the set of background pixels of I [31]. The Euclidean distance transforms $d^+ : I \to \mathbb{R}$ and $d^- : I \to \mathbb{R}$ of the image I displayed in Figure 4(a) are displayed in Figures 5(a) and 5(b) respectively.

$$d^+(p) = \min_{q \in \text{Fore}(I)} \|p - q\| \tag{8}$$

$$d^-(p) = \min_{q \in \text{Back}(I)} \|p - q\| \tag{9}$$

Given the distance transforms $d^+ : I \to \mathbb{R}$ and $d^- : I \to \mathbb{R}$, the functions $f^+ : \mathcal{K} \to \mathbb{R}$ and $f^- : \mathcal{K} \to \mathbb{R}$ are defined in Equations 10 and 11 respectively.

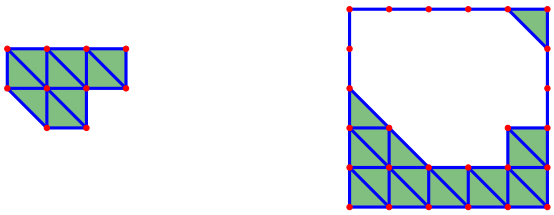

(a) (b)

Figure 6: The 0 sublevel sets of $f^+ : \mathcal{K} \to \mathbb{R}$ and $f^- : \mathcal{K} \to \mathbb{R}$ corresponding to the simplicial complex displayed in Figure 4(b) are displayed in (a) and (b) respectively.

These functions assign to each simplex in $\mathcal{K}$ the maximum of the functions d^+ and d^- respectively evaluated on the corresponding 0-simplex faces. These functions induce filtrations which model the positive and negative distance functions respectively. The 0 sublevel sets of f^+ and f^- corresponding to the simplicial complex displayed in Figure 4(b) are displayed in Figures 6(a) and 6(b) respectively.

$$f^+(\sigma) = \max_{\tau \in \sigma} d^+(\tau) \tag{10}$$

$$f^-(\sigma) = \max_{\tau \in \sigma} d^-(\tau) \tag{11}$$

Given the filtrations induced by the functions d^+ and d^- the corresponding persistence diagrams are computed using the method of [28]. Briefly, this method involves encoding each filtration as a matrix and performing a matrix reduction. As discussed above, these persistence diagrams model the persistence diagrams corresponding to the functions $L_t^{S^+}$ and $L_t^{S^-}$ respectively. That is, the sublevel sets of the positive and negative distance functions respectively. These persistence diagrams are denoted $\text{Pers}_p(L_t^{S^+})$ and $\text{Pers}_p(L_t^{S^-})$ respectively.

4. Results

In this section we demonstrate the ability of the proposed shape model to accurately model multi-scale topological features of single and multiple compo-

nent shapes. The remainder of this section is structured as follows. Section 4.1 describes the baseline models against which the proposed model is evaluated. Sections 4.2 and 4.3 present an evaluation of the proposed model with respect to single and multiple component shapes respectively.

4.1. Baseline Models

To evaluate the model we considered the following three baseline models. The first baseline model corresponds to the persistent homology of a filtration which models the sublevel sets of the unsigned distance function $U(.)$ defined in Equation 5; that is, $\text{Pers}_p(L_t^U)$. This is a commonly employed method to constructing a filtration for a given data and therefore represents a suitable baseline [30]. As discussed in section 3.2, the unsigned and positive distance functions are equivalent.

The second baseline model corresponds to the model proposed by Di Fabio et al. [22]. As described in section 2, this model employs two filtrations defined on the shape boundary. The first filtration considers the distance to a vector pointing in a principle direction and passing through the mean point. The second filtration considers the distance to a plane orthogonal to this vector and passing through the mean point. This model assumes the shape in question is represented in terms of its boundary. All shapes used in this work are initially represented as binary images. We therefore extracted the shape boundaries for all shapes before applying the model. To illustrate this model consider the shape in Figure 1(a) for which the corresponding boundary is represented in Figure 7(a). In this example the vector pointing in the principle direction is parallel to the x-axis while the plane orthogonal to this vector is a vector parallel to the y-axis. The persistence diagrams corresponding to the first and second filtrations are displayed in Figures 7(b) and 7(c) respectively.

The third baseline model corresponds to the model proposed by Turner et al. [19]. As described in section 2, this model computes a set of persistence diagrams where each corresponds to a filtration defined on the shape with respect to distance in a specified direction. In this work we used two directions corre-

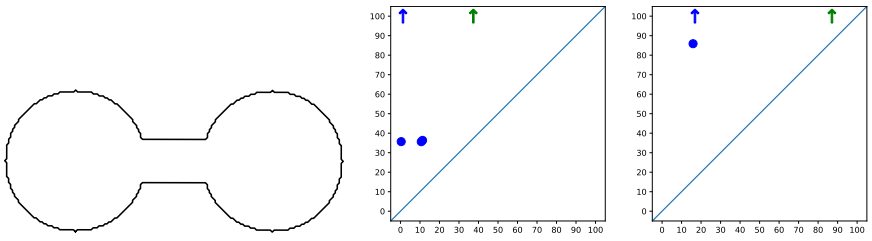

(a) (b) (c)

Figure 7: The boundary corresponding to the shape of Figure 1(a) is displayed in (a). The persistence diagrams corresponding to the first and second filtrations in the model by Di Fabio et al. [22] are displayed in (b) and (c) respectively. Elements of the 0-dimensional and 1-dimensional persistence diagrams are represented using blue circles and green triangles respectively. Elements of these persistence diagrams that appear but do not disappear are determined to disappear at a value of ∞ and are represented by blue and green vertical arrows respectively.

sponding to the first and second principal components. To illustrate this model consider again the shape in Figure 1(a) for which the corresponding boundary is represented in Figure 8(a). In this example the first principal component is parallel to the x-axis while the second principal component is parallel to the y-axis. The persistence diagrams corresponding to the first and second principal components are displayed in Figures 8(b) and 8(c) respectively.

4.2. Single Component Shapes

In many cases the use of a filtration which models the sublevel sets of the unsigned distance function does not accurately model the multi-scale topological features. To illustrate this point with respect to single component shapes consider the two shapes represented in Figures 1(a) and 1(b). As discussed in the introduction to this article, from a multi-scale perspective the topological features of these shapes can be considered to be distinct. The persistence diagrams $\text{Pers}_p(L_t^U)$ for these shapes are displayed in Figures 9(a) and 9(b) respectively. It is evident that the persistence diagrams corresponding to both shapes are equal and therefore cannot discriminate between the shapes in ques-

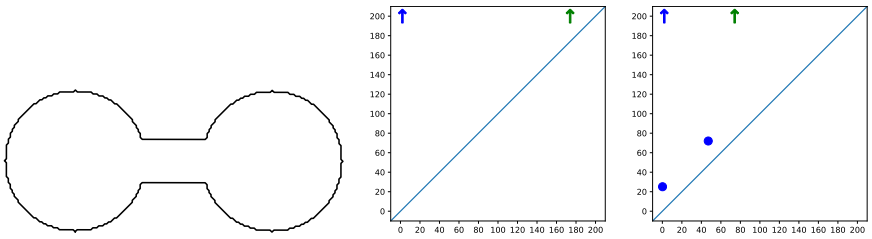

(a) (b) (c)

Figure 8: The boundary corresponding to the shape of Figure 1(a) is displayed in (a). The persistence diagrams corresponding to the first and second principal components in the model by Turner et al. [19] are displayed in (b) and (c) respectively. Elements of the 0-dimensional and 1-dimensional persistence diagrams are represented using blue circles and green triangles respectively. Elements of these persistence diagrams that appear but do not disappear are determined to disappear at a value of ∞ and are represented by blue and green vertical arrows respectively.

tion. That is, the persistence diagrams indicate that in the case of both shapes a single path-connected component appears at a distance of 0 to the data and does not subsequently disappear. They also indicate that in the case of both shapes no one-dimensional holes appear. This demonstrates that, in this case, the persistence diagrams corresponding to an unsigned distance function $U(.)$ fail to accurately model multi-scale topological features.

The proposed model of multi-scale topological features overcomes the above limitation by computing a pair of persistence diagrams $\text{Pers}_p(L_t^{S^+})$ and $\text{Pers}_p(L_t^{S^-})$ corresponding to the distance functions S^+ and S^- respectively. Relative to persistence diagrams corresponding to the unsigned distance function $U(.)$, this pair models additional multi-scale topological features which facilitate more accurate discrimination. The persistence diagrams $\text{Pers}_p(L_t^{S^+})$ and $\text{Pers}_p(L_t^{S^-})$ corresponding to the shapes of Figures 1(a) and 1(b) are displayed in Figure 3. As described in section 3.2, these persistence diagrams discriminate between the shapes in question.

To evaluate the performance of the proposed shape model with respect to a larger and more complex set of shapes we considered the MPEG-7 shape dataset

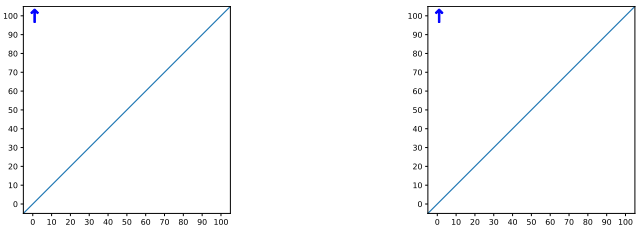

(a) (b)

Figure 9: The persistence diagrams $\text{Pers}_p(L_t^U)$ for the shapes in Figures 1(a) and 1(b) are displayed in (a) and (b) respectively. In each figure elements of $\text{Pers}_0(L_t^U)$ and $\text{Pers}_1(L_t^U)$ are represented using blue circles and green triangles respectively. Elements of $\text{Pers}_0(L_t^U)$ that appear but do not disappear are determined to disappear at a value of ∞ and are represented by a blue vertical arrow.

[32]. This dataset consists of 70 distinct shape categories with 20 individuals shapes per category to give a total of 1,400 shapes. Two sample shapes in this data set are displayed in Figures 10(a) and 11(a). In order to reduce the computation time required to run experiments, we considered a subset of this dataset corresponding to all 70 shape categories but only 10 individuals shapes per category. The high computational complexity results from having to compute the q-Wasserstein distance a large number of times. Toward making the proposed and benchmark models robust to differences in object scale, we normalized the size of each image such that the corresponding number of foreground object pixels was approximately 4,000.

We evaluated the proposed and baseline models with respect to the task of shape retrieval on the above dataset. For a given model, we selected the k closest shapes to each shape in the dataset. The 2-Wasserstein distance was used to measure distances. For example, Figures 10 and 11 display the 4 most similar shapes to a given shape as determined by all models. The proposed and baseline models of Di Fabio et al. [22] and Turner et al. [19] performed equally well with respect to the retrieval example of Figure 10. On the other hand, the baseline models of Di Fabio et al. [22] and Turner et al. [19] performed

(a)

(b) 2.11-0.0-54.92-22.38

(c) 4.06-0.0-42.11-25.23

(d) 5.84-0.0-40.79-40.75

(e) 6.01-0.0-32.30-28.14

(f) 14.63-0.0-163.35-149.76

(g) 13.38-0.0-164.84-148.04

(h) 14.60-0.0-166.17-150.18

(i) 19.83-0.0-152.20-138.90

(j) 6.20-0.0-28.81-16.66

(k) 6.01-0.0-32.30-28.14

(l) 5.84-0.0-40.79-40.75

(m) 9.54-0.0-41.32-24.68

(n) 6.20-0.0-28.81-16.66

(o) 6.01-0.0-32.30-22.38

(p) 5.84-0.0-40.79-25.23

(q) 9.54-0.0-41.32-28.14

Figure 10: For the query shape in (a), the four most similar shapes as determined by the proposed, unsigned distance, Di Fabio et al. [22] and Turner et al. [19] models are displayed in rows two, three, four and five respectively. In each row shapes are ordered from most to least similar from left to right. The caption under each shape gives the respective dash separated distances to the query shape.

(a)

(b) 8.01-3.97-53.06-34.78

(c) 24.17-8.80-105.85-112.55

(d) 24.96-9.35-90.23-110.58

(e) 25.25-9.35-189.89-167.73

(f) 8.01-3.97-53.06-34.78

(g) 30.58-7.52-93.18-87.19

(h) 31.58-8.07-116.05-155.66

(i) 30.48-8.41-122.79-158.15

(j) 8.01-3.7-53.06-34.78

(k) 26.32-9.31-73.05-73.85

(l) 33.32-9.83-75.83-74.32

(m) 25.37-9.05-76.52-64.9

(n) 8.01-3.7-53.06-34.78

(o) 25.37-9.05-76.52-64.9

(p) 26.32-9.31-73.05-73.85

(q) 41.90-11.84-89.61-79.92

Figure 11: For the query shape in (a), the four most similar shapes as determined by the proposed, unsigned distance, Di Fabio et al. [22] and Turner et al. [19] models are displayed in rows two, three, four and five respectively. In each row shapes are ordered from most to least similar from left to right. The caption under each shape gives the respective dash separated distances to the query shape.

slightly better than the proposed model with respect to the retrieval example of Figure 11. For both retrieval examples the unsigned distance baseline model performed the worst. For the example in Figure 10 this can be attributed to the fact that this model fails to model the fact that the query shape corresponds to two larger scale connected components connected by a smaller scale path. This is a defining feature of the shape in question. Instead, the model determines a large number of shapes as being identical, that is having distance value of zero, to the query shape. A consequence of this is that an arbitrary subset of these are determined to be the k closest shapes.

For values of k from 1 to 10, the corresponding precision and recall values for the four models over the 700 shapes are displayed in Figure 12(a). These values demonstrate that the model by Di Fabio et al. [22] outperformed all other models with respect to shape retrieval on this dataset. One explanation for this is that using the principle direction to control filtration provides some additional shape specification information that is helpful to the shape retrieval task. However, as we shall see in the next experiment in section 4.3, this dependence on the principle direction can become counter-productive.

4.3. Multiple Component Shapes

To illustrate that the proposed shape model is applicable to multiple component shapes consider the three shapes displayed in Figure 2. As discussed in the introduction to this article, from a multi-scale perspective the topological features of the shapes in Figures 2(a) and 2(b) can be considered similar while those of the shape in Figure 2(c) can be considered distinct. The persistence diagrams $\text{Pers}_p(L_t^{S^+})$ and $\text{Pers}_p(L_t^{S^-})$ corresponding to the three shapes of Figure 2 are displayed in Figure 13. Note that, two triangles exists at the location (0,35) in the persistence diagrams of Figures 13(d) and 13(f). It is evident that the persistence diagrams corresponding to these shapes accurately model the corresponding multi-scale topological features. For example, the persistence diagrams $\text{Pers}_p(L_t^{S^+})$ of Figures 13(a) and 13(c) indicate that, from a multi-scale perspective, the shapes in Figures 2(a) and 2(b) consist of a single significant

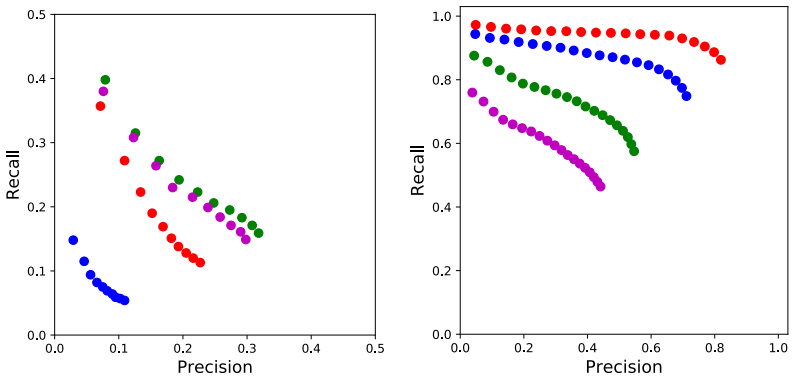

(a) (b)

Figure 12: The precision and recall values for the single and multiple component retrieval tasks are displayed in (a) and (b) respectively. Points for the proposed, unsigned distance, Di Fabio et al. [22] and Turner et al. [19] models are represented by red, blue, green and magenta points respectively.

path-connected component. That is, Figures 13(a) and 13(c) illustrate that for both shapes $\text{Pers}_0(L_t^{S^+})$ contains a single point with significant persistence. In both cases this point is represented by a blue arrow in the corresponding figure. On the other hand, the persistence diagrams $\text{Pers}_p(L_t^{S^+})$ of Figure 13(e) indicate that, from a multi-scale perspective, the shape in Figure 2(c) consists of two significant path-connected components. These points are represented by a blue circle and blue arrow in the corresponding figure.

We evaluated the proposed shape model on a multiple component version of the MPEG-7 shape dataset which contains in total 3,621 shapes [32]. A subset of 620 shapes in this dataset consists of 31 individual shapes plus 9 distorted, 5 rotated and 5 scaled versions of each shape. A small distortion of a shape, such as a small affine transformation, can result in topological changes which would be considered to be very distinct unless a multi-scale perspective is considered. For example two connected components which are spatially close may form a single connected component following the application of a small distortion transformation. Figure 14 displays one of the individual shapes in the dataset

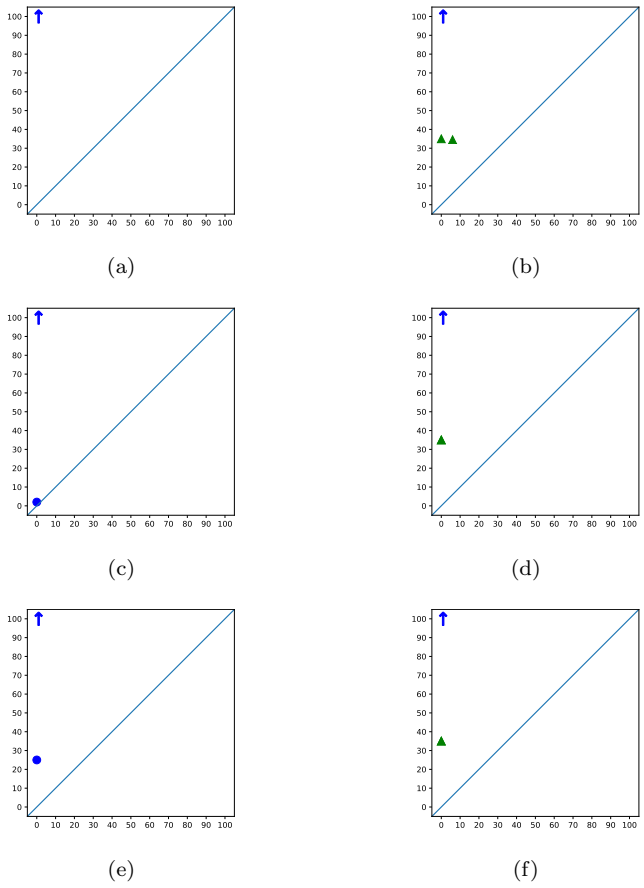

Figure 13: The persistence diagrams $\text{Pers}_p(L_t^{S^+})$ and $\text{Pers}_p(L_t^{S^-})$ corresponding to the shape of Figure 2(a) are displayed in (a) and (b) respectively. The persistence diagrams $\text{Pers}_p(L_t^{S^+})$ and $\text{Pers}_p(L_t^{S^-})$ corresponding to the shape of Figure 2(b) are displayed in (c) and (d) respectively. The persistence diagrams $\text{Pers}_p(L_t^{S^+})$ and $\text{Pers}_p(L_t^{S^-})$ corresponding to the shape of Figure 2(c) are displayed in (e) and (f) respectively. In each figure elements of $\text{Pers}_0(.)$ and $\text{Pers}_1(.)$ are represented using blue circles and green triangles respectively. Elements of $\text{Pers}_0(.)$ that appear but do not disappear are determined to disappear at a value of ∞ and are represented by a blue vertical arrow. Note that, two triangles exists at the location (0,35) in the persistence diagrams of (d) and (f).

(a) (b) (c) (d)

Figure 14: Distorted, rotated and scaled versions of the shape in (a) are displayed in (b), (c) and (d) respectively.

plus a subset of the corresponding transformed versions.

Using the same methodology employed for single component shapes, we evaluated the proposed and baseline models with respect to the task of shape retrieval on the above dataset. For values of k from 1 to 20, the corresponding precision and recall values for the four models over the 620 shapes are displayed in Figure 12(b). These values demonstrate that the proposed model outperformed the baselines models respect to shape retrieval on this dataset. Figures 15 and 16 display the 4 most similar shapes to a given shape in the dataset as determined by all models. It is evident that the proposed model outperforms the baseline models with respect to these shapes. The authors believe that the relatively poor performance of the Di Fabio et al. [22] and Turner et al. [19] baseline models can in part be attributed to the fact that they are defined with respect to the shape boundary and therefore struggle to differentiate between the interior and exterior of a shape. The other cause for their relatively poor performance is their reliance on principle directions. However, the estimation of such directions can become unreliable for compact or rotationally symmetric shapes, and in such situations becomes overly-sensitive to artifacts caused by the digitization process or by noise [33]. We note that a significant number of the shapes in the MPEG-7 dataset are compact and/or rotationally symmetric.

To further demonstrate the performance of the proposed shape model we considered another subset of the above multiple component dataset correspond-

(a)

(b) 5.7-3.2-85.2-74.8

(c) 6.7-3.0-154.6-251.7

(d) 7.0-3.1-86.4-73.2

(e) 7.4-3.7-84.0-71.5

(f) 7.6-2.8-29.1-38.1

(g) 7.8-2.8-74.1-68.5

(h) 8.5-2.9-79.2-66.9

(i) 6.7-3.0-154.6-251.7

(j) 7.6-2.8-29.1-38.1

(k) 27.5-17.1-71.3-79.0

(l) 7.8-2.8-74.1-68.5

(m) 27.8-17.6-75.1-90.4

(n) 7.6-2.8-29.1-38.1

(o) 8.5-2.9-79.2-66.9

(p) 7.6-3.2-77.2-66.9

(q) 35.8-20.8-95.0-68.5

Figure 15: For the query shape in (a), the four most similar shapes as determined by the proposed, unsigned distance, Di Fabio et al. [22] and Turner et al. [19] models are displayed in rows two, three, four and five respectively. In each row shapes are ordered from most to least similar from left to right. The caption under each shape gives the respective dash separated distances to the query shape.

(a)

(b) 6.9-4.1-760.2-1441.1

(c) 17.4-11.0-923.2-141.1

(d) 19.9-12.2-885.2-129.2

(e) 20.8-14.4-1040.6-706.8

(f) 6.9-4.1-760.2-1441.1

(g) 17.4-11.0-923.2-141.1

(h) 19.9-12.2-885.2-129.2

(i) 57.1-12.3-947.9-2311.6

(j) 83.3-30.2-657.5-88.2

(k) 21.4-14.0-739.5-4102.9

(l) 6.9-4.1-760.2-1441.1

(m) 97.7-36.6-769.7-1464.5

(n) 28.7-20.4-1013.8-128.8

(o) 19.9-12.2-885.2-129.2

(p) 22.5-15.7-111.3-134.9

(q) 81.2-48.7-1325.2-141.7

Figure 16: For the query shape in (a), the four most similar shapes as determined by the proposed, unsigned distance, Di Fabio et al. [22] and Turner et al. [19] models are displayed in rows two, three, four and five respectively. In each row shapes are ordered from most to least similar from left to right. The caption under each shape gives the respective dash separated distances to the query shape.

ing to the first 200 shapes in the dataset. Unlike the previous subset considered, this subset is not formally structured and instead contains random shapes some of which have a varying number of distorted versions. On this subset we performed the task of retrieval using the same methodology described above. Figure 17 displays the three most similar shapes to four query shapes as determined by the proposed model. It is evident that for the three query shapes in Figures 17(a), 17(e) and 17(i), the model retrieves shapes which are similar to the query shape. However, for the query shape in Figure 17(m) the model does not retrieve shapes which are similar to the query shape. This can be attributed to the fact that although the query shape has distinctive features these features are not topological in nature.

5. Conclusions

This paper proposes a novel shape model which is demonstrated to accurately model multi-scale topological features. The proposed model is applicable to both single and multiple component shapes and, to the authors knowledge, is the first shape model to consider multi-scale topological features of multiple component shapes.

The proposed model was evaluated both qualitatively and quantitatively against three suitable baseline models using a number of datasets. This evaluation demonstrates that the proposed model fails to outperform one of the baseline models with respect to the task of modelling single component shapes. However, it outperforms both baseline models with respect to the task of modelling multiple component shapes. The authors believe there exists scope to develop a novel shape model which integrates the benefits of both the proposed and baseline models.

Although in this paper we consider the specific problem of modelling two dimensional shapes represented as binary images, the proposed model has the potential to be applied to other problem instances. This includes modelling three dimensional shapes represented as polygon meshes and modelling arbitrary

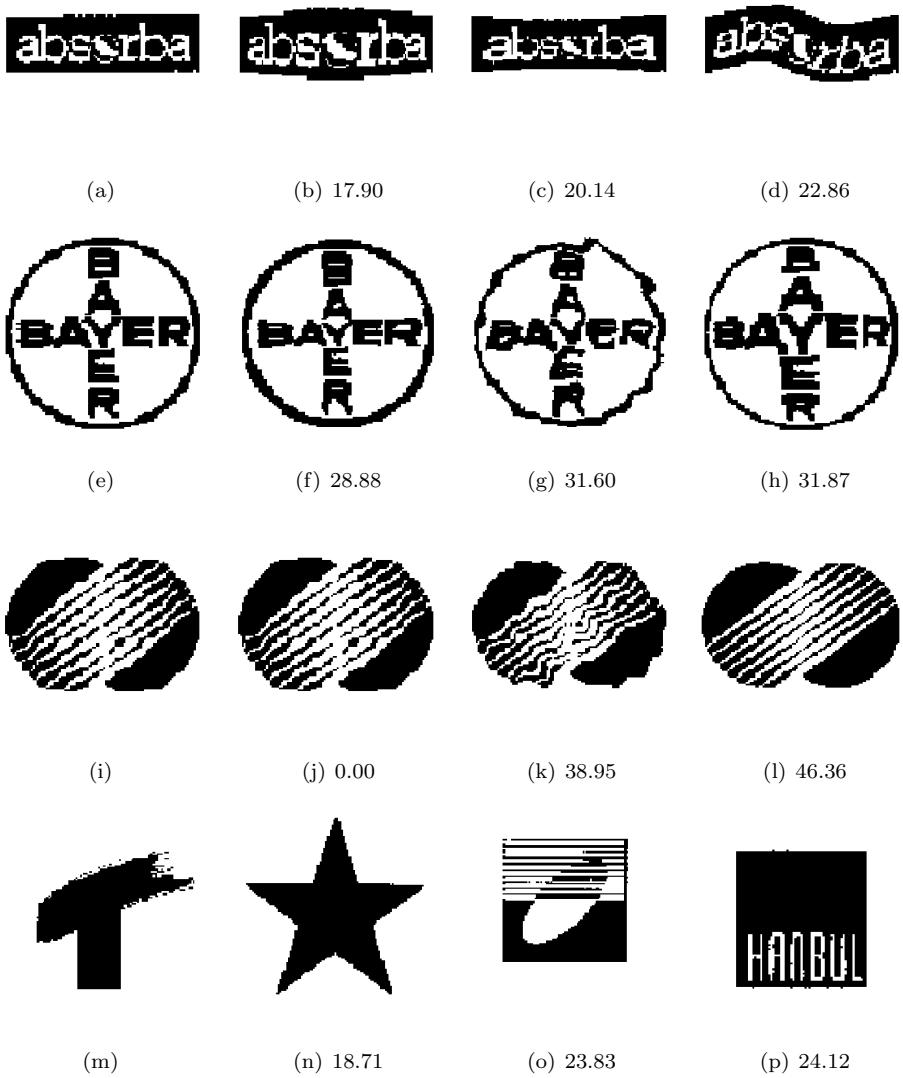

(a) (b) 17.90 (c) 20.14 (d) 22.86

(e) (f) 28.88 (g) 31.60 (h) 31.87

(i) (j) 0.00 (k) 38.95 (l) 46.36

(m) (n) 18.71 (o) 23.83 (p) 24.12

Figure 17: The first column of each row contains a query shape. The three most similar shapes from most to least similar as determined by the proposed model are displayed in the second, third and fourth columns respectively. The caption under each shape gives the corresponding distance to the query shape as determined by the proposed model rounded to two decimal places.

dimensional shapes represented as point clouds.

References

[1] D. Madsen, M. Lüthi, A. Schneider, T. Vetter, Probabilistic joint face-skull modelling for facial reconstruction, in: IEEE Conference on Computer Vision and Pattern Recognition, 2018, pp. 5295–5303 (2018).

[2] J. C. Baker-LePain, K. R. Luker, J. A. Lynch, N. Parimi, M. C. Nevitt, N. E. Lane, Active shape modeling of the hip in the prediction of incident hip fracture, Journal of Bone and Mineral Research 26 (3) (2011) 468–474 (2011).

[3] N. Correll, K. E. Bekris, D. Berenson, O. Brock, A. Causo, K. Hauser, K. Okada, A. Rodriguez, J. M. Romano, P. R. Wurman, Analysis and observations from the first Amazon picking challenge, IEEE Transactions on Automation Science and Engineering 15 (1) (2018) 172–188 (2018).

[4] F. P. Kuhl, C. R. Giardina, Elliptic fourier features of a closed contour, Computer Graphics and Image Processing 18 (3) (1982) 236–258 (1982).

[5] T. Rauber, A. Steiger-Garcao, Shape description by UNL Fourier features – an application to handwritten character recognition, in: International Conference on Pattern Recognition, 1992, pp. 466–469 (1992).

[6] R. Mukundan, K. Ramakrishnan, Moment Functions in Image Analysis – Theory and Applications, World Scientific, 1998 (1998).

[7] J. Flusser, B. Zitova, T. Suk, Moments and moment invariants in pattern recognition, John Wiley & Sons, 2009 (2009).

[8] P. Corcoran, P. Mooney, A. Winstanley, A Convexity Measure for Open and Closed Contours, in: British Machine Vision Conference, 2011 (2011).

[9] P. L. Rosin, Measuring shape: ellipticity, rectangularity, and triangularity, Machine Vision and Applications 14 (3) (2003) 172–184 (2003).

[10] S. Belongie, J. Malik, J. Puzicha, Shape context: A new descriptor for shape matching and object recognition, in: Advances in neural information processing systems, 2001, pp. 831–837 (2001).

[11] F. Mokhtarian, A. K. Mackworth, A theory of multiscale, curvature-based shape representation for planar curves, IEEE Transactions on Pattern Analysis & Machine Intelligence (8) (1992) 789–805 (1992).

[12] C. Asian, S. Tari, An axis-based representation for recognition, in: International Conference on Computer Vision Volume 1, Vol. 2, 2005, pp. 1339–1346 (2005).

[13] K. B. Eom, Shape recognition using spectral features, Pattern Recognition Letters 19 (2) (1998) 189 – 195 (1998).

[14] Z. You, A. K. Jain, Performance evaluation of shape matching via chord length distribution, Computer vision, graphics, and image processing 28 (2) (1984) 185–198 (1984).

[15] J. Zunic, P. L. Rosin, V. Ilic, Disconnectedness: A new moment invariant for multi-component shapes, Pattern Recognition 78 (2018) 91–102 (2018).

[16] P. Corcoran, C. B. Jones, Modelling topological features of swarm behaviour in space and time with persistence landscapes, IEEE Access 5 (2017) 18534–18544 (2017).

[17] J. Curry, R. Ghrist, M. Robinson, Euler calculus with applications to signals and sensing, in: Symposia in Applied Mathematics, 2012 (2012).

[18] Z. Zhou, Y. Huang, L. Wang, T. Tan, Exploring generalized shape analysis by topological representations, Pattern Recognition Letters 87 (2017) 177–185 (2017).

[19] K. Turner, S. Mukherjee, D. M. Boyer, Persistent homology transform for modeling shapes and surfaces, Information and Inference: A Journal of the IMA 3 (4) (2014) 310–344 (2014).

[20] J. Curry, S. Mukherjee, K. Turner, How many directions determine a shape and other sufficiency results for two topological transforms, arXiv preprint arXiv:1805.09782 (2018).

[21] B. Di Fabio, C. Landi, Persistent homology and partial similarity of shapes, Pattern Recognition Letters 33 (11) (2012) 1445–1450 (2012).

[22] B. Di Fabio, M. Ferri, Comparing persistence diagrams through complex vectors, in: International Conference on Image Analysis and Processing, Springer, 2015, pp. 294–305 (2015).

[23] M. Zeppelzauer, B. Zieliński, M. Juda, M. Seidl, A study on topological descriptors for the analysis of 3d surface texture, Computer Vision and Image Understanding 167 (2018) 74–88 (2018).

[24] A. Cerri, B. Di Fabio, F. Medri, Multi-scale approximation of the matching distance for shape retrieval, in: Computational Topology in Image Context, Springer, 2012, pp. 128–138 (2012).

[25] J. Munkres, Elements of Algebraic Topology, Westview Press, 1996 (1996).

[26] H. Edelsbrunner, J. Harer, Computational topology: an introduction, American Mathematical Society, 2010 (2010).

[27] H. Edelsbrunner, J. Harer, Persistent homology – a survey, Contemporary Mathematics 453 (2008) 257–282 (2008).

[28] A. Zomorodian, G. Carlsson, Computing persistent homology, Discrete & Computational Geometry 33 (2) (2005) 249–274 (2005).

[29] M. Kerber, D. Morozov, A. Nigmetov, Geometry helps to compare persistence diagrams, Journal of Experimental Algorithmics 22 (2017) 1–4 (2017).

[30] F. Chazal, B. Fasy, F. Lecci, B. Michel, A. Rinaldo, L. Wasserman, Robust topological inference: Distance to a measure and kernel distance, Journal of Machine Learning Research 18 (159) (2018) 1–40 (2018).

[31] R. Fabbri, L. D. F. Costa, J. C. Torelli, O. M. Bruno, 2D Euclidean distance transform algorithms: a comparative survey, ACM Computing Surveys 40 (1) (2008) 2 (2008).

[32] M. Bober, MPEG-7 visual shape descriptors, IEEE Transactions on Circuits and Systems for Video Technology 11 (6) (2001) 716–719 (2001).

[33] J. Zunic, P. L. Rosin, L. Kopanja, On the orientability of shapes, IEEE Transactions on Image Processing 15 (11) (2006) 3478–3487 (2006).